



Comparative study of the thermal diffusivity of SiO₂-Au nanoparticles in water base

Angel Netzahual Lopantzi¹ · José Francisco Sánchez Ramírez² · José Luis Jiménez Pérez¹

Received: 3 December 2019 / Accepted: 27 January 2020 / Published online: 10 February 2020
© Springer-Verlag GmbH Germany, part of Springer Nature 2020

Abstract

Two SiO₂-Au nanoparticles were prepared. Silicon dioxide (SiO₂) structures with average size of 143 and 90 nm were synthesized using the sol-gel method. Gold (Au) nanoparticles of ~5 nm were deposited using the deposition-precipitation process on each dielectric platform. The concentration of silanol groups of SiO₂ spheres was obtained. The size and form of SiO₂, Au and SiO₂-Au nanoparticles were evaluated by transmission electron microscopy (TEM). The TEM micrographs confirmed the size and spherical form for SiO₂ and Au nanoparticles with high monodispersity, the decoration of SiO₂ spheres with metallic nanoparticles was also confirmed. The reflectance spectrum revealed a decreased of reflectivity around 516 nm for SiO₂-Au structures, the decrease of reflectance was associated with the presence of gold nanoparticles on dielectric spheres. The SiO₂-Au structures (at different mass 0.1–0.6 mg/ml) were dispersed in deionized water. Thermal diffusivity of SiO₂-Au particles in water was studied using the thermal lens (TL) spectroscopy. The results revealed an increase in thermal diffusivity as the SiO₂-Au concentration was increased. The thermal property was independent on the size of the SiO₂ spheres used.

Keywords Thermal diffusivity · SiO₂ spheres · Au nanoparticles

1 Introduction

Nowadays, the nanostructures formed of a platform of SiO₂ and metal nanoparticles over surface are materials that are attracting interest of recent research, because they provide stability, without aggregation. The SiO₂ is a cheap and abundant material in nature, SiO₂ nanospheres are synthesized easily with high monodispersity [1], versatile to bond with other materials. SiO₂ of 385 nm decorated with Ag nanoparticles (5–10 nm) was prepared by Chen et al. [2] using seed-mediated growth process. Recently, the strategy of electrostatic attraction between [Ag(NH₃)₂]⁺ ions with the hydroxyl (–OH[–]) groups on the surface of silica particles

was used [3], thus SiO₂ (220 nm) decorated with silver nanoparticles (10–50 nm) were prepared.

The synthesis of SiO₂ decorated with Au nanoparticles was reported using several routes, by immersion [4] and evaporation method [5]. Sputtering deposition and dewetting process for synthesis of SiO₂ nanowires decorated with gold nanoparticles were used by Ruffino and Grimaldi in 2013 [6]. The one-step synthesis using irradiation electron technique was reported, the process involved prepares a precursor solution of HAuCl₄·3H₂O-PVP-containing SiO₂ spheres with average size ~240 nm, and the irradiation of 6 MeV electrons at 1.5 × 10¹⁵ e[–]/cm² [7]. On the other hand, chemical route was used, with the anchored amino groups in the surface of SiO₂ structures to bond metallic species [8].

The application of the SiO₂ structures decorated with gold nanoparticles is wide, since it has been used as carriers DNA [9]. It also served as a biosensor device, because antibodies of bovine serum albumin (anti-BSA) were immobilized in SiO₂-Au structure [10]. In addition, the SiO₂-Au structure showed an enhancement of light absorption around to the frequency of surface plasmon resonance (SRP) of metallic nanoparticles [5]. Phantagare and coworkers [7] prepared surface-enhanced Raman scattering (SERS) substrate-based 3 nm Au nanoparticles embedded on SiO₂ spheres (240 nm),

✉ Angel Netzahual Lopantzi
lopantzi_@hotmail.com

¹ Unidad Profesional Interdisciplinaria en Ingeniería Y Tecnologías Avanzadas-Instituto Politécnico Nacional, Av. Instituto Politécnico Nacional No. 2580, Col. Barrio La Laguna Ticomán, Del. Gustavo A. Madero, C.P. 07340 México, D.F., México

² Instituto Politécnico Nacional-CIBA. Ex-Hacienda San Juan Molino Carretera Estatal Tecuexcomac-Tepetitla, Km 1.5, Tlaxcala, C.P. 90700 México, México

the authors detect concentration limit $\sim 10^{-18}$ M of thiabendazole, crystal violet and 4-aminophenol. The SiO₂ and Au structures separated was also reported, Kim and coworkers reported that SiO₂ nanoparticles to dose of 200 µg/ml was compatible in NIH/3T3 cells [11], gold nanoparticles (35 nm) amplified the light scattering in cancer oral cell lines [12]. Au nanoparticles with average size = 5 nm polymer coated (polyethylene glycol) were synthesized [13], the metallic particles showed biocompatibility in murine monocytic macrophages. Also, the Au nanostructures have photodynamic or photothermal therapy applications; using an appropriate wavelength lasers, the light is converted to heat [14, 15], the heat is released to environment. The rate of heat transfer is related to thermal diffusivity parameter, for this thermal parameter in SiO₂ spheres values of 15×10^{-4} cm²/s [16] and gold nanoparticles 26×10^{-4} cm²/s [17] was reported.

The applications of the SiO₂ particles aforementioned are highly dependent on the physicochemical properties. For this reason, in this work, SiO₂ decorated with Au nanostructures was prepared using two different sizes of dielectric platform. Also, the thermal diffusivity of SiO₂-Au was studied using thermal lens spectroscopy.

2 Experimental

2.1 Sample preparation

The reagents used for the preparation of the SiO₂-Au spheres were tetraethyl orthosilicate (TEOS, 99%), ammonium hydroxide (NH₄OH, 28–30% as ammonia NH₃), (3-aminopropyl) triethoxysilane (APTES), tetrachloroauric acid (HAuCl₄·3H₂O, 99.99%), sodium borohydride (NaBH₄ 98%) and sodium citrate dihydrate [OHC (COONa) (CH₂·COONa)₂·2H₂O, 99%]. All were acquired from Sigma Aldrich. Methanol (CH₃OH 99%), ethanol (C₂H₅OH 99%) and sodium hydroxide (NaOH 99%) were obtained from the chemical company J.T. Baker. All chemicals were of analytical grade and used without further purification. Deionized water was employed for preparing the solutions (Millipore system with resistivity 18.2 M Ω cm).

2.1.1 Synthesis of SiO₂ and SiO₂-Au structures

Two different sizes of SiO₂ spherical structures were prepared using the Stöber method 1968 [1]. The method consists in the hydrolysis and condensation of TEOS with ammonium hydroxide as a catalyst agent and ethanol as solvent. The SiO₂ spheres were synthesized employing the TEOS as molecular precursor of SiO₂. In an Erlenmeyer flask (65 × 110 mm), 60 ml of a solution containing ethanol (14.4 mol/l), TEOS (0.037 mol/l), water (5.9 mol/l) and

ammonia (0.98 and 0.49 mol/l) were mixed. The solution was subjected to vigorous agitation to overnight at 300 rpm and room temperature. The resulting colloidal suspension was washed by centrifugation (12,000 rpm for 15 min) and rinsed with ethanol/water at a volumetric ratio 1/1, repeating the process at least five times.

0.3 g of SiO₂ spheres (143 and 90 nm) dispersed in 1 ml deionized water were surface functionalized with -NH₂ amino groups, the decoration of SiO₂ spheres with Au nanoparticles was made according to Kah et al. [8]. Briefly, 10 ml of a gold precursor solution containing HAuCl₄ and NaOH to concentrations of 6.35 and 0.1 mol/l, respectively, was prepared; the last solution was mixed with 0.25 ml of the solution of amino-functionalized SiO₂ spheres. The mixture was then heated at 70 °C for 30 min under vigorous stirring to the homogeneous deposition of gold hydroxide Au(OH)₃ on the surface of SiO₂ spheres. The product was washed by centrifugation at 8,000 rpm and dried at 60 °C. 0.015 g of SiO₂-Au(OH)₃ were dissolved in 20 ml of water and mixed with 10.5 ml of NaBH₄ (6.6 mol/l) and 5.25 ml of sodium citrate (10 mol/l) to reduce Au(OH)₃ in Au⁰ over SiO₂ [18]. The samples were washed by centrifugation 8,000 rpm/h, rinsed with deionized water at least five times and dried at 60 °C. All process was repeated for each size of SiO₂.

3 Characterization

Spectroscopic and microscopic techniques were used for the morphological characterization of SiO₂ and SiO₂-Au nanostructures. UV-Vis spectroscopy (spectrophotometer Genesys 10S, Thermo scientific) measurements were made on samples dispersed in water. Reflectance spectroscopy by UV-Vis-NIR (Cary 5000) through the diffuse reflectance technique, the samples were characterized in powder. For FTIR measurements, the samples were characterized in the range of 400–4,000 cm⁻¹. Transmission electron microscopy (TEM, model JEOL JEM 1010) for TEM each of the colloidal samples was deposited on a copper grid (covered with a FORMVAR film) until the solvent was evaporated at room temperature. EDS (Energy Dispersive X-Ray Spectroscopy) spectra of samples were obtained from SEM/EDS microscope model JEOL JSM IT300.

The concentration of silanol groups was determined through alkali neutralization method [19]. Briefly, in a flask, 0.2 g of sample was mixed with 50 ml (0.05 M) of solution of NaOH, the mixture was stirred for 12 h. The sample was centrifuged and 10 ml of supernatant was titrated against 0.05 M of solution HCl, using 0.1% phenolphthalein as indicator. The concentration of total hydroxyl groups (X mmol/g) per unit grams of silica was estimated according to the following formula:

$$X = \frac{(B - A) \times 0.05 \times 5}{W}, \tag{1} \quad m = \frac{\omega_p}{\omega_e}, \tag{4}$$

where *A* is the amount (ml) of HCl need for neutralization, *B* refer to ml of HCl consumed in a blank. *W* is the mass of sample, in this work 0.2 g was tested.

3.1 Thermal lens

Thermal diffusivity values was obtained using thermal lens technique. This technique involves the incidence of an excitation laser with a Gaussian profile on the sample causing the absorbed energy transformed into heat. In this case, a temperature gradient is established, and a change of refractive index. When a second test laser is passed in the sample, an effect of focusing or defocusing of the light beam is caused, this phenomenon produced is called thermal lens [20, 21].

The mode-mismatched dual-beam experimental arrangement of thermal lens spectrometry is observed in Fig. 1, the sample was exposed to an excitation laser (Ar⁺-Xe), where it generates a local temperature increase, also the probe beam (He-Ne) passes through the sample propagating until photodiode.

The experimental data were adjusted using the theoretical Eq. (1) [22]:

$$I(t) = I(0) \left[1 - \frac{\theta}{2} \tan^{-1} \left(\frac{2mV}{[(1 + 2m)^2 + V^2]^{\frac{t_c}{2t}} + 1 + 2m + V^2} \right) \right], \tag{2}$$

where

$$V = \frac{Z_1}{Z_c}, \tag{3}$$

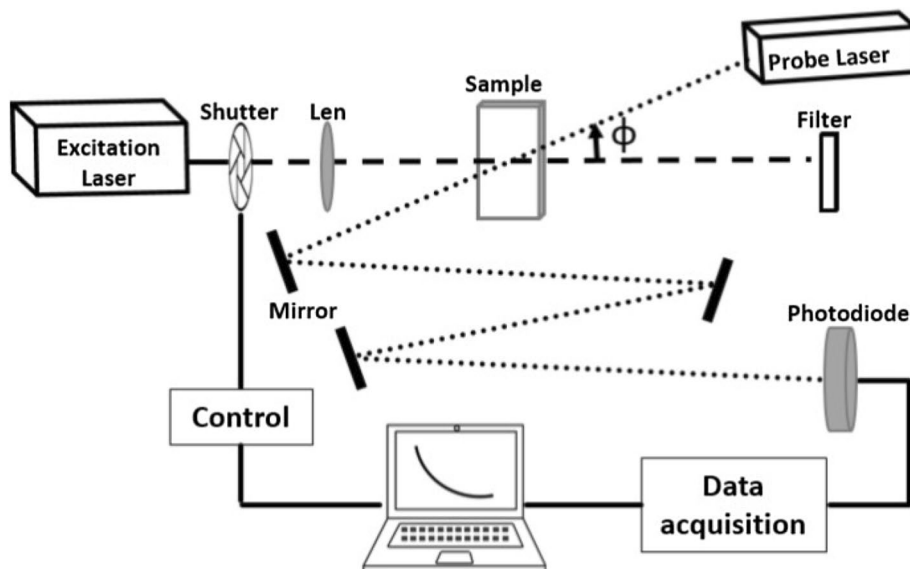
$$\theta = -\frac{P_e A_e l_o}{k \lambda_p} \left(\frac{dn}{dT} \right), \tag{5}$$

where *I*(*t*) is the time dependent of test beam to detector, *I*(0) is the initial value of *I*(*t*) for *t* zero; *θ* corresponds to phase shift thermal induced of probe beam after passes through sample; *Z_c* (12.89 cm) is the confocal distance of probe beam; *Z₁* (8 cm) belongs to distance of the sample to the position of the minimum radius of the test beam; *ω_e* and *ω_p* are the spot size of excitation laser and probe beam, respectively, to the sample; *k* and *D* are the conductivity and thermal diffusivity of sample; *P_e* is the incident power; *A_e* is the optical absorption coefficient to wavelength of the excitation laser *λ_e*; *λ_p* refers to beam-probe wavelength; *l_o* is the sample thickness; *dn/dT* is the refractive index-dependent temperature of sample.

$$D = \frac{\omega_e^2}{4t_c}, \tag{6}$$

where *t_c* is the characteristic thermal time constant with *D* = *k*/(*ρc_p*), where *ρ* is the density and *c_p* is the heat capacity of the sample. The experimental value of the excitation laser waist is *ω_e* = 40 μm. Thus, adjusting the equation *I*(*t*) to the experimental data as a function-time is possible obtain thermal diffusivity *D* (Eq. 5) from *t_c* as adjustable parameter. For thermal diffusivity measurements, SiO₂-Au samples in water were subjected in ultrasound to ensure redispersion correct of particles.

Fig. 1 Representation of the experimental arrangement of thermal lens spectroscopy in mode-mismatched dual beam



4 Results and discussion

The formation and size of SiO₂ structures were investigated by TEM microscopy. Figure 2a, b shows the TEM micrographs of SiO₂ particles formed using the sol–gel method (1968). Structures well defined with spherical shape were observed. Approximately, 60 particles were counted and size distribution histograms were obtained. Insets of Fig. 2a, b showed the average size were 143 and 90 nm employing ammonium hydroxide to concentrations of 0.98 and 0.49 mol/l, respectively. According to standard deviation of the histograms, the samples synthesized have high monodispersity ($\sigma < 22\%$). The concentrations of catalyst employed and average size of spheres obtained are consistent with early reported by other authors [23, 24].

The SiO₂ particles were characterized by EDS spectroscopy. The elemental composition is shown in the Fig. 3a, b. In both samples, the oxygen and silicon were recorded without any contaminant. According to the elemental analysis, the atomic percent of oxygen was higher in SiO₂ particles 90 nm (Fig. 3b) than silica spheres of 143 nm (Fig. 3a). The observation can be justified as follows: the oxygen forms siloxane (Si–O–Si) and silanol (Si–OH) bonds, but in small silica particles, the –OH level is high reported by Nabeshi et al. [25], for this reason, the SiO₂ of 90 nm recorded higher oxygen content.

The SiO₂ spheres were characterized by FTIR. The typical spectra IR of SiO₂ spheres are shown in the Fig. 4. The IR peaks (455, 550, 800, 1080, and 1200 cm⁻¹) related with vibrations of siloxane groups can be observed. The bands at 1640 and 3362 cm⁻¹ are associated to vibrations hydroxyl

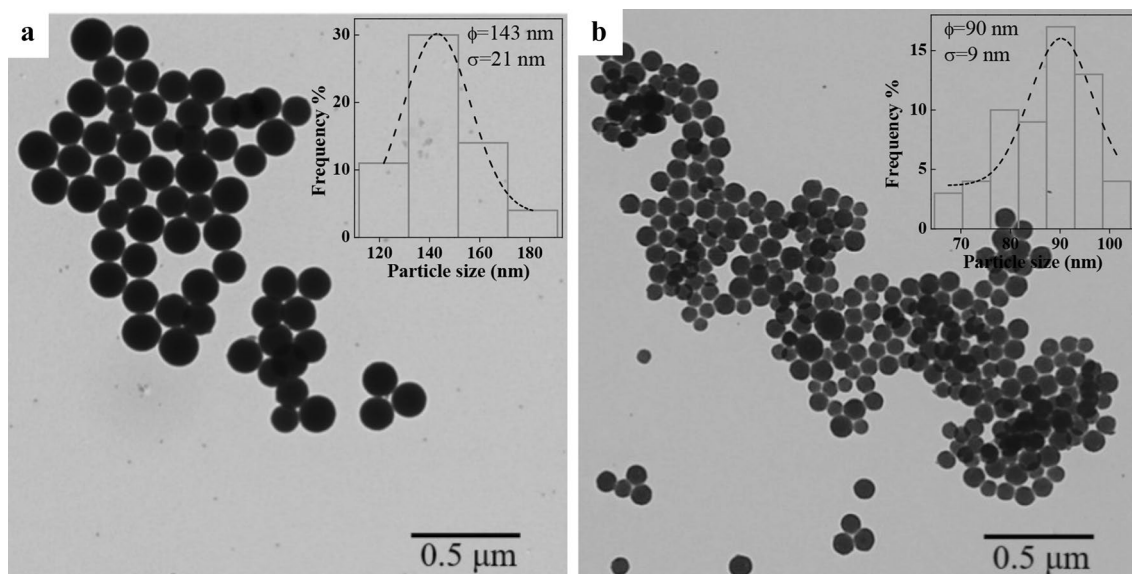


Fig. 2 TEM micrographs of SiO₂ particles synthesized using **a** 0.98 and **b** 0.49 mol/l of catalyst. *Insets:* size distribution histograms

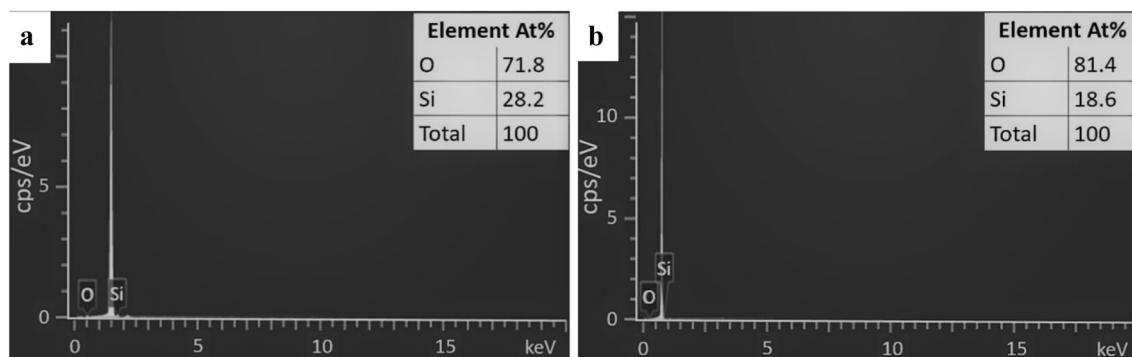


Fig. 3 EDS spectra of silica particles of **a** 143 nm and **b** 90 nm

Fig. 4 Infrared absorbance of SiO₂ particles synthesized using **a** 0.98 and **b** 0.49 mol/l of catalyst

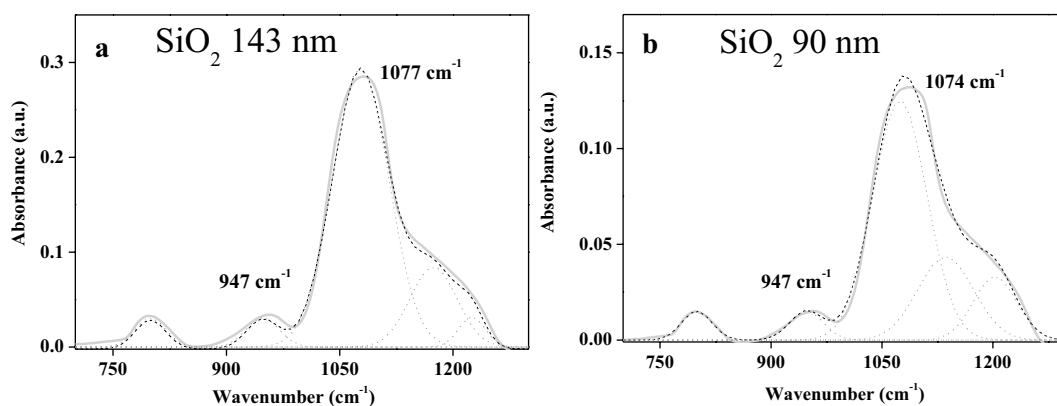
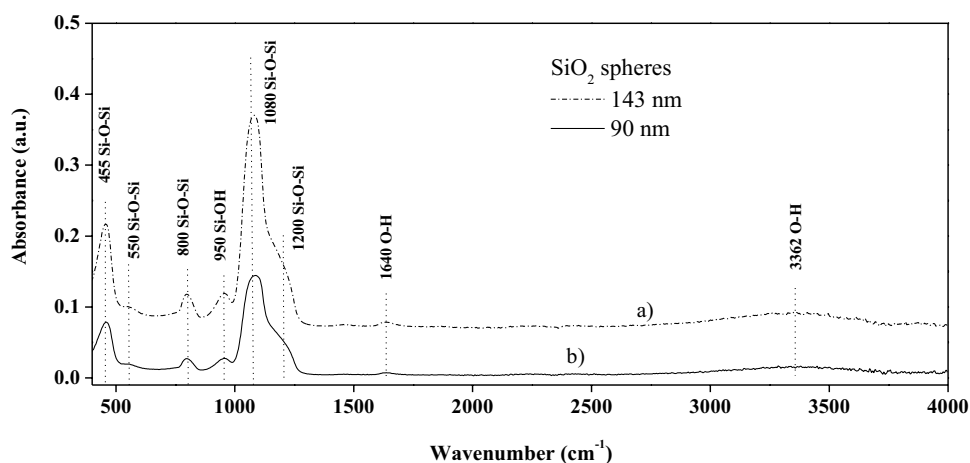


Fig. 5 Deconvoluted IR absorption spectra of SiO₂ spheres with an average size of **a** 143 nm and **b** 90 nm. The intense bands at 1077 and 947 cm⁻¹ were used to calculate the ratio $I_{\text{Si-O-Si}}/I_{\text{Si-OH}}$

-OH groups. Finally, the IR band around 950 corresponds to vibration of silanol groups [18].

The concentration of silanol groups can be estimated using the bands 1080 cm⁻¹ and 950 cm⁻¹ related to siloxane and silanol groups, respectively [26]. In this work, the deconvolution of the absorption spectra in the region 700–1300 cm⁻¹ was realized. In Fig. 5, five Gaussian subbands (dot lines), the sum (dash lines), and the experimental spectra (gray line) of two samples are shown. The high intense band around 1074 cm⁻¹ is related with the transverse optical (TO) asymmetric stretching vibration of bond Si-O-Si. The intensity of last band was compared with the intensity of silanol band at 947 cm⁻¹. The results are shown in Table 1, for SiO₂ of 143 nm, a ratio value ($I_{\text{Si-O-Si}}/I_{\text{Si-OH}}$) of 16.4 was recorded, and for SiO₂ particles of 90 nm, an intensity ratio of 13.5 was obtained. According to the literature [27], a lower value in the ratio $I_{\text{Si-O-Si}}/I_{\text{Si-OH}}$, the concentration of silanol groups is high. Therefore, this suggests that SiO₂ spheres of 90 nm containing higher concentration of silanol groups than 143 nm.

Table 1 Ratio values $I_{\text{Si-O-Si}}/I_{\text{Si-OH}}$ of two different sizes of SiO₂ spheres

| Particle size (nm) | Position Si-OH | Intensity Si-OH | Position Si-O-Si | Intensity Si-O-Si | Intensity ratio $I_{\text{Si-O-Si}}/I_{\text{Si-OH}}$ |
|--------------------|----------------|-----------------|------------------|-------------------|---|
| 143 | 947 | 1.68 | 1077 | 27.55 | 16.4 |
| 90 | 947 | 0.85 | 1074 | 11.48 | 13.5 |

The concentration of silanol groups was also determined by alkaline neutralization method. A process drying during 2 h was carried out in the samples for eliminated adsorbed -OH. The results were 0.40 and 0.44 mmol/g of silanol groups for SiO₂ spheres of 143 and 90 nm, respectively, as shown in Table 2. The silanol values were similar to that reported by Rhaman et al. [28]. The lower Si-OH concentration was recorded in dielectric spheres of 90 nm, the result was according with FTIR spectrum analysis.

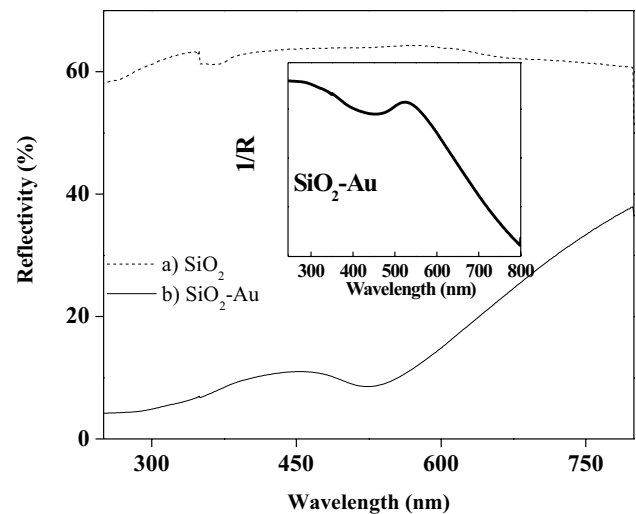
The SiO₂-Au nanostructures were investigated by TEM microscopy. In Fig. 6a, b, spherical gold nanoparticles

Table 2 Concentration of silanol groups of two SiO₂ samples

| Particle size (nm) | Concentration of silanol groups (mmol/g) | |
|--------------------|--|--------------------|
| | Average | Standard deviation |
| 143 | 0.40 | 0.006 |
| 90 | 0.44 | 0.005 |

deposited on surface SiO₂ at different sizes were observed. Approximately, 30 gold nanoparticles on each dielectric platform were counted and size distribution histograms were obtained. The histograms of insets in the Fig. 6a, b revealed an average size of 5.1 and 5.4 nm for gold nanoparticles attached over SiO₂ spheres with size of 143 and 90 nm, respectively, these values were similar to that reported by Kah and coworkers [8]. The standard deviation of metallic nanoparticles revealed a high monodispersity in the size distribution. The Au interparticle distance was estimated using Image J software, the distances were from 3 to 10 nm for all samples of SiO₂ decorated with Au nanoparticles. Therefore, TEM micrographs proved gold nanoparticle immobilization over SiO₂ spheres, using chemical synthesis quickly and efficiently in the setting of SiO₂ in-situ.

The SiO₂ spheres with size of 143 nm were used for reflectance spectroscopy characterization. Figure 7 presents reflectivity spectra in the 250–800 nm range of SiO₂ spheres bare (spectrum a) and SiO₂ spheres decorated with ~5 nm of gold nanoparticles (spectrum b). Only for SiO₂ spheres, 60%

**Fig. 7** Reflectance spectra for **a** 143 nm of SiO₂ spheres before and **b** after of decorated with gold nanoparticles. *Inset:* is the inverse of the reflectivity

of the reflectivity was recorded, i.e., is a highly reflective material. After the decorated process, a change of reflectivity in the SiO₂-Au nanoparticles was recorded; in this case, a decay of reflectance percent to 10% around of 516 nm, phenomenon associated to the presence of gold nanoparticles on SiO₂ spheres. Similar results to the observed by Covertino et al. [5]. It is worth noting that the inverse of the reflectivity spectrum (inset in the Fig. 7) had a behavior similar to the extinction coefficient of only gold nanoparticles dispersed

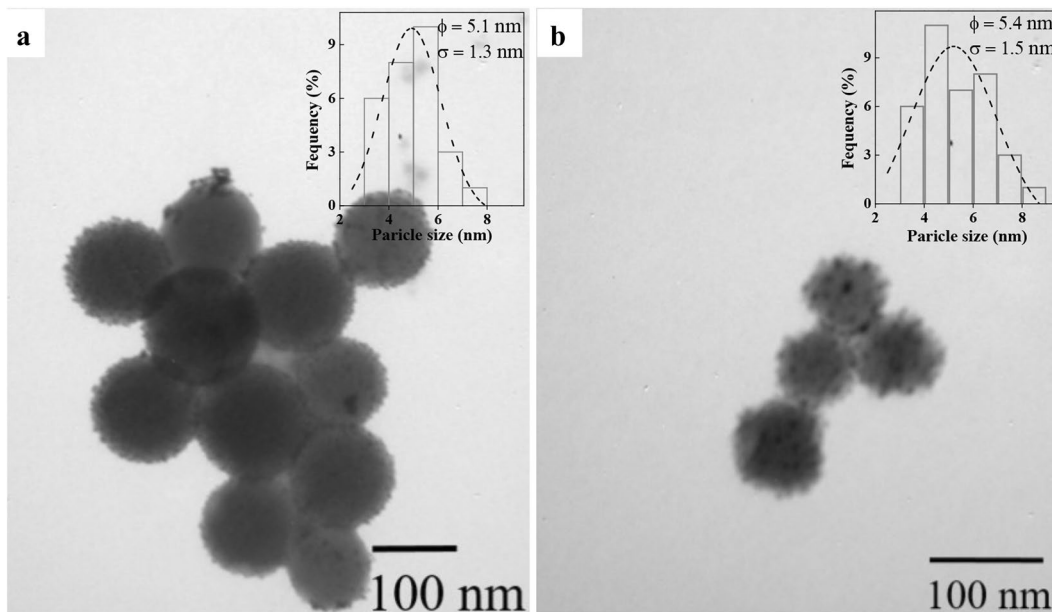
**Fig. 6** TEM micrographs of gold nanoparticles deposited on SiO₂ spheres **a** 143 and **b** 90 nm. *Insets:* size distribution histograms.

Fig. 8 Spectra UV-Vis for SiO₂ decorated with gold nanoparticles using dielectric platform of **a** 143 and **b** 90 nm

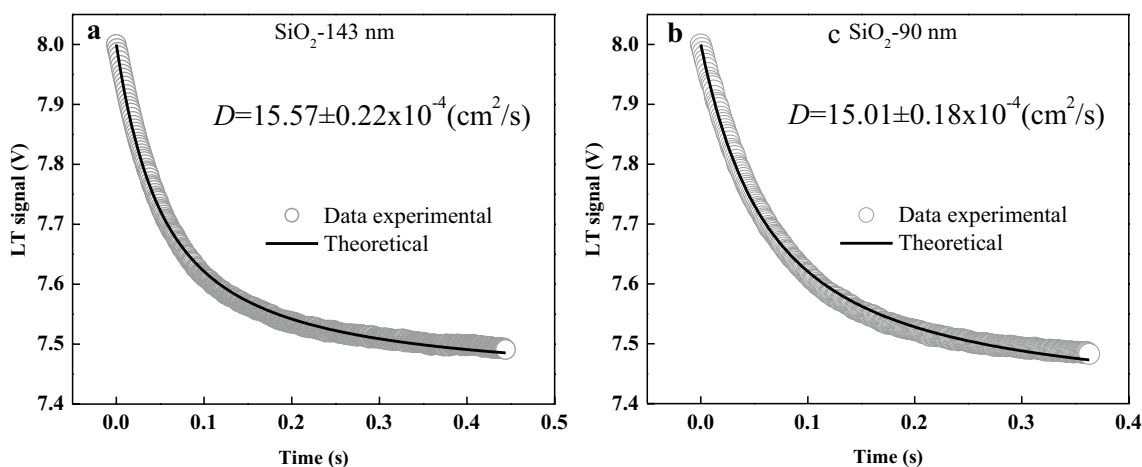
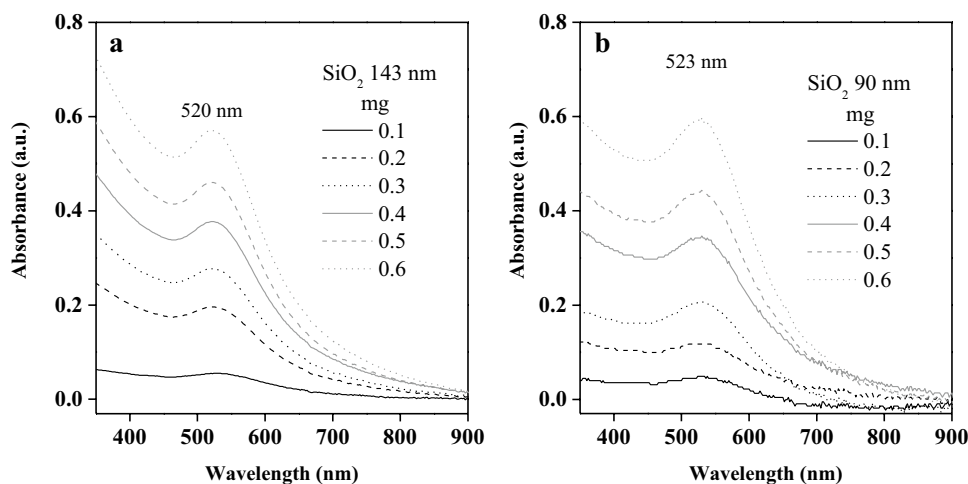


Fig. 9 Thermal lens signal to SiO₂ decorated with gold nanoparticles using dielectric platform **a** 143 and **b** 90 nm

in water [5]. Therefore, the results confirmed the attachment gold nanoparticles on SiO₂ spheres.

The SiO₂-Au nanostructures were dried to obtain powder, then the powder was diluted in 1 ml of deionized water at concentrations from 0.1 to 0.6 mg. Six different samples for each size of SiO₂ were obtained, the samples were measured by spectroscopy UV-Vis. The results revealed absorption bands (Fig. 8a, b) to 520 and 523 nm for gold nanoparticles with a size 5.1 and 5.4 nm, respectively. To larger size of the particle, there will be a larger shift towards greater wavelengths, these red shift phenomenon in the absorption is consistent with other reports [7]. An increase of absorbance was also recorded according to the mass of SiO₂ decorated with gold nanoparticles, shown in Fig. 8.

Figure 9 shows typical spectra of thermal lens evolution vs time of SiO₂-Au structures dispersed in water at 0.1 mg mass, the theoretical curve of the spectra was calculated with Eq. 2 and fits experimental data appropriately, in addition,

Table 3 TL parameters of SiO₂ decorated with gold nanoparticles using SiO₂ of 143 nm

| Concentration (mg/ml) | Thermal diffusivity of SiO ₂ -Au size 143 nm | | |
|-----------------------|---|----------------------------------|---------------------------|
| | $D (\times 10^{-4} \text{ cm}^2/\text{s})$ | $t_c (\times 10^{-3} \text{ s})$ | $\theta (\times 10^{-2})$ |
| 0.1 | 15.57 ± 0.22 | 3.85 ± 0.05 | 1.39 ± 0.03 |
| 0.2 | 17.52 ± 0.18 | 3.41 ± 0.04 | 2.01 ± 0.15 |
| 0.3 | 19.99 ± 0.27 | 3.02 ± 0.04 | 0.76 ± 0.04 |
| 0.4 | 21.50 ± 0.50 | 2.73 ± 0.03 | 1.67 ± 0.06 |
| 0.5 | 23.99 ± 0.24 | 2.50 ± 0.02 | 1.21 ± 0.13 |
| 0.6 | 25.87 ± 0.46 | 2.32 ± 0.04 | 1.07 ± 0.21 |

thermal time in which the thermal lens induced in the sample is recorded in milliseconds according to earlier reports [29].

The thermal diffusivity values of SiO₂-Au structures dispersed in water are observed in Tables 3 and

Table 4 TL parameters obtained for SiO₂-Au nanostructures using a platform of 90 nm

| Concentration (mg/ml) | Thermal diffusivity of SiO ₂ -Au size 90 nm | | |
|-----------------------|--|-----------------------------|-------------------------------|
| | D ($\times 10^{-4}$ cm ² /s) | t_c ($\times 10^{-3}$ s) | θ ($\times 10^{-2}$) |
| 0.1 | 15.01 \pm 0.18 | 4.01 \pm 0.05 | 5.62 \pm 1.27 |
| 0.2 | 17.06 \pm 0.21 | 3.51 \pm 0.04 | 8.27 \pm 0.81 |
| 0.3 | 19.12 \pm 0.19 | 3.13 \pm 0.03 | 9.03 \pm 0.82 |
| 0.4 | 21.96 \pm 0.26 | 2.86 \pm 0.04 | 8.59 \pm 0.44 |
| 0.5 | 24.55 \pm 0.29 | 2.44 \pm 0.03 | 5.91 \pm 0.31 |
| 0.6 | 27.31 \pm 0.06 | 2.20 \pm 0.05 | 4.80 \pm 0.88 |

4. It is worth mentioned that the values are an average of 10 measures for each sample. The thermal diffusivity results registered an increase according to the concentration of SiO₂-Au nanostructures from $15.57 \pm 0.22 \times 10^{-4}$ to $25.87 \pm 0.46 \times 10^{-4}$ cm²/s for 143 nm of SiO₂. The thermal diffusivity from $15.01 \pm 0.18 \times 10^{-4}$ to $27.30 \pm 0.18 \times 10^{-4}$ cm²/s for 90 nm of SiO₂ was recorded. The adjustable parameters θ and t_c obtained from the best fit of Eq. (2) to TL experimental data are also shown. The SiO₂ decorated with gold nanoparticle structures synthesized in this work recorded higher thermal diffusivity values than separated structures; i.e., only SiO₂ spheres (of 300 nm) dispersed in deionized water to 0.37 mg/ml with thermal value of 14.96×10^{-4} cm²/s [19]. On the other hand, at 0.1 mg gold nanoparticles (≈ 16 nm) dispersed in 1 ml of deionized water recorded a thermal diffusivity of 14.96×10^{-4} cm²/s [30], in this work at same concentration (0.1 mg/ml), the SiO₂-Au was recorded 15.57×10^{-4} cm²/s. Thus, thermal diffusivity values of SiO₂-Au in water provide a high heat transfer to surrounding environment. It is well documented that SiO₂-Au nanostructures have been not only used as gene carrier or biosensors [9, 10], but also can be used as material thermal delivery in thermal therapy against cancer cell.

It was shown that the gold nanoparticles anchored over SiO₂ spheres change optic properties of dielectric platform, for example, a decrease in reflectance and increased absorbance associated to surface plasmon resonant showed in Figs. 7 and 8, similar results to reported by Covertino et al. [5]. In SiO₂ decorated with Au nanoparticles, an improvement in light absorption was recorded, associated to the presence of gold nanoparticles on SiO₂ structures, the improvement was not registered in SiO₂ without decorated. The enhanced light absorption is because the light inside each SiO₂-Au structure is trapped, i.e., light trapping, this optic phenomenon was schematized by Netzahual Lopantzi et al. [18]. The heat transfer to water was measured by thermal diffusivity using thermal lens spectroscopy. According

to Tables 3 and 4, thermal diffusivity values were similar between SiO₂-Au structures using different dielectric platform. A possible explanation of this thermal observation between the SiO₂-Au nanostructures is described below. The chemical characterization by EDS, FTIR and alkaline neutralization helped to know contained of silanol groups in each SiO₂ sphere. The silanol groups is very important, because they are responsible for attaching amino groups and incorporation of metals. In this work, the silanol concentration was 0.40 and 0.44 mmol/g for SiO₂ spheres of 143 and 90 nm, respectively. Despite this difference in silanol groups, this suggests that the two silica particles have the approximately the same capacity to attach gold nanoparticles and thermal diffusivity values similar. Moreover, the size, shape and interparticle distance of Au nanoparticles on silica particles were almost the same. Therefore, the thermal diffusivity values between two SiO₂-Au were similar. According to results reported by Rhaman et al. [31], both SiO₂ particles (143 and 90 nm) has approximately 11 -OH groups per nm². The thermal results also revealed an increase of thermal diffusivity according to concentration of SiO₂-Au was increased. This is because thermal diffusivity depends on factors as size and concentration of the gold nanoparticles due to the surface-to-volume ratio [32, 33].

5 Conclusion

The SiO₂ spheres with a controlled size (143 and 90 nm) were synthesized, these dielectric structures served as platform to anchored gold nanoparticles confirmed by TEM, UV-Vis and reflectance spectroscopy. The thermal diffusivity values were independent of size of SiO₂ sphere employed. Because the silanol groups, size and distance between gold nanoparticles, in the two different SiO₂ platforms are almost the same. The thermal results revealed an increase of thermal diffusivity as the concentration of SiO₂-Au was increased. The SiO₂-Au structures dispersed in water offer a higher value in thermal diffusivity than separated structures, i.e., only SiO₂ spheres or gold nanoparticles dispersed in water with equivalent sizes at similar concentrations, the combination of dielectric and metallic materials increased heat transfer to environment, in this case, the water measured by thermal lens spectroscopy. The SiO₂-Au nanostructures synthesized in this work have potential applications as SERS substrate, as carrier administration targeted system, according to the interparticle separation, there is sufficient space for the Au nanoparticle functionalization with target molecules. Finally, in thermal area, SiO₂-Au nanoparticles could be used in the photodynamic treatment against cancer cells.

References

- W. Stöber, A. Fink, Controlled growth of monodisperse silica spheres in the micron size range. *J Colloid Interface Sci* **26**(1), 62–69 (1968). [https://doi.org/10.1016/0021-9797\(68\)90272-5](https://doi.org/10.1016/0021-9797(68)90272-5)
- C. Kuang-Hsiu, P. Ying-Chih Pu, C. Kao-Der, L. Yi-Fan, L. Chia-Ming, Y. Jien-Wei, S. Han-C, H. Yung-Jung, Ag-Nanoparticle-decorated SiO₂ nanospheres exhibiting remarkable plasmon-mediated photocatalytic properties. *J Phys Chem C* **116**(35), 19039–19045 (2012). <https://doi.org/10.1021/jp306555j>
- M. Nur-Kamilah, W. Mohd Afiq, W. Mohd Khalik, A. A. Azmi, Synthesis and characterization of silicasilver core-shell nanoparticles. *Malays Anal Sci Soc* **43**(2), 290–299 (2009). <https://doi.org/10.17576/mjas-2019-2302-13>
- G. Zhong-Ze, R. Horie, S. Kubo, Y. Yamada, A. Fujishima, O. Sato, Fabrication of a metal-coated three-dimensionally ordered macroporous film and its application as a refractive index sensor. *Angew Chem* **41**(7), 1153–1156 (2002). [https://doi.org/10.1002/1521-3757\(20020402\)114:7%3c1201:AID-ANGE1201%3e3.0.CO;2-0](https://doi.org/10.1002/1521-3757(20020402)114:7%3c1201:AID-ANGE1201%3e3.0.CO;2-0)
- A. Convertino, M. Cusunà, F. Martelli, M. Manera, R. Rella, Silica nanowires decorated with metal nanoparticles for refractive index sensors: three-dimensional metal arrays and light trapping at plasmonic resonances. *J Phys Chem* **118**(1), 685–690 (2014). <https://doi.org/10.1021/jp411743p>
- F. Ruffino, M.G. Grimaldi, Au nanoparticles decorated SiO₂ nanowires by dewetting on curved surfaces: facile synthesis and nanoparticles–nanowires sizes correlation. *J Nanopart Res* **15**, 1–17 (2013). <https://doi.org/10.1007/s11051-013-1909-6>
- A.B. Phantagare, S.D. Dhole, S.S. Dahiwal, V.N. Bhoraskar, Ultra-high sensitive substrates for surface enhanced Raman scattering, made of 3 nm gold nanoparticles embedded on SiO₂ nanospheres. *Appl Surf Sci* **441**, 744–753 (2018). <https://doi.org/10.1016/j.apsusc.2018.02.057>
- J.C.Y. Kah, N. Phonthammachai, R.C.Y. Wang, J. Song, T. White, S. Mhaisalkar, I. Ahmadb, C. Shepparda, M. Olivo, Synthesis of gold nanoshells based on the deposition–precipitation process. *Gold Bull* **41**(1), 23–36 (2008). <https://doi.org/10.1007/BF03215620>
- L. Wang, T. Cheang, S. Wang, Z. Hu, Z. Xing, W. Qu, A. Xu, Monodisperse Au/aminosilica composite nanospheres: facile one-step synthesis and their applications in gene transfection. *J Mater Res* **27**(18), 2425–2430 (2012). <https://doi.org/10.1557/jmr.2012.218>
- A. Colombelli, M.G. Manera, A. Taurino, M. Catalano, A. Convertino, R. Rella, Au nanoparticles decoration of silica nanowires for improved optical bio-sensing. *Sens Actuators B Chem* **226**, 589–597 (2016). <https://doi.org/10.1016/j.snb.2015.11.075>
- I. Kim, E. Joachim, H. Choi, K. Kim, Toxicity of silica nanoparticles depends on size, dose, and cell type. *Nanomed Nanotechnol Biol Med* **11**(6), 1407–1416 (2015). <https://doi.org/10.1016/j.nano.2015.03.004>
- I.H. El-Sayed, X. Huang, M.A. El-Sayed, Surface plasmon resonance scattering and absorption of anti-EGFR antibody conjugated gold nanoparticles in cancer diagnostics: applications in oral cancer. *Nano Lett* **5**(5), 829–834 (2005). <https://doi.org/10.1021/nl050074e>
- A. Orlando, M. Colombo, D. Prosperi, F. Corsi, A. Panariti, I. Rivolta, M. Masserini, E. Cazzaniga, Evaluation of gold nanoparticles biocompatibility: a multiparametric study on cultured endothelial cells and macrophages. *J Nanopart Res* **18**(3), 58 (2016). <https://doi.org/10.1007/s11051-016-3359-4>
- P. García-Calavia, G. Bruce, L. Pérez-García, D.A. Russel, Photosensitizer-gold nanoparticle conjugates for photodynamic therapy of cancer. *Photochem Photobiol Sci* **17**, 1534–1552 (2018). <https://doi.org/10.1039/C8PP00271A>
- M. Khosroshahi, M.S. Nourbakhsh, In vitro skin wound soldering using SiO₂/Au nanoshells and a diode laser. *Med Laser Appl* **26**(1), 35–42 (2011). <https://doi.org/10.1016/j.mla.2010.06.001>
- A.H. Abdelrazek, O.A. Alawi, S.N. Kazi, N. Yusoff, Z. Chowdhury, A.D. Sarhan, A new approach to evaluate the impact of thermophysical properties of nanofluids on heat transfer and pressure drop. *Int Commun Heat Mass Transfer* **95**, 161–170 (2018). <https://doi.org/10.1016/j.icheatmasstransfer.2018.05.002>
- E. Shahriar, Y.W.M. Mat, R. Zamiri, The effect of nanoparticle size on thermal diffusivity of gold nano-fluid measured using thermal lens technique. *J Euro Opt Soc Rapid Publ* **8**, 13026 (2013). <https://doi.org/10.2971/jeos.2013.13026>
- A. Netzahual-Lopantzi, J.F. Sánchez-Ramírez, J.L. Jiménez-Pérez, D. Cornejo-Monroy, G. López-Gambo, Z.N. Correa-Pacheco, Study of the thermal diffusivity of nanofluids containing SiO₂ decorated with Au nanoparticles by thermal lens spectroscopy. *Appl Phys A* **125**, 588 (2019). <https://doi.org/10.1007/s00339-019-2891-3>
- S. Yuaga, M. Okabayashi, H. Ohno, K. Suzuki, K. Kusumoto, U.S. Patent 4, 764,497, 1988
- J.L. Jiménez-Pérez, J.F. Sánchez-Ramírez, D. Cornejo-Monroy, R. Gutiérrez-Fuentes, J.A. Pescador-Rojas, A. Cruz-Orea, C. Jacinto, Photothermal study of two different nanofluids containing SiO₂ and TiO₂ semiconductor nanoparticles. *Int J Thermophys* **33**(1), 69–79 (2012). <https://doi.org/10.1007/s10765-011-1139-z>
- R. Carbajal-Valdez, J.L. Jiménez-Pérez, A. Cruz-Orea, Z.N. Correa-Pacheco, M. Alvarado-Noguez, I.C. Romero-Ibarra, J.G. Mendoza-Álvarez, Thermal properties of centrifuged oils measured by alternative photothermal techniques. *Thermochim Acta* **657**, 66–71 (2017). <https://doi.org/10.1016/j.tca.2017.09.014>
- J. Shen, R. Lowe, R.D. Snook, A model for cw laser induced mode-mismatched dual-beam thermal lens spectrometry. *Chem Phys* **165**(1–3), 385–396 (1992). [https://doi.org/10.1016/0301-0104\(92\)87053-C](https://doi.org/10.1016/0301-0104(92)87053-C)
- T. Matsoukas, E. Gulari, Dynamics of growth of silica particles from ammonia-catalyzed hydrolysis of tetra-ethyl-orthosilicate. *J Colloid and Interface Sci* **124**(1), 252–261 (1988). [https://doi.org/10.1016/0021-9797\(88\)90346-3](https://doi.org/10.1016/0021-9797(88)90346-3)
- D. Cornejo-Monroy, J.A. Pescador-Rojas, J.F. Sánchez-Ramírez, J.L. Herrera-Pérez, Nanoesferas monodispersas de SiO₂: síntesis controlada y caracterización. *Revista Superficies y Vacío* **22**(3), 44–48 (2009)
- H. Nabeshi, T. Yoshikawa, K. Matsuyama, Y. Nakazato, S. Tochigi, T. Kondoh, T. Hirai, T. Akase, K. Nagano, Y. Abe, Y. Yoshioka, H. Kamada, N. Itoh, S. Thunoda, Y. Tsutsumi, Amorphous nanosilica induce endocytosis-dependent ROS generation and DNA damage in human keratinocytes. *Part Fibre Toxicol* **8**(1), 1–10 (2011). <https://doi.org/10.1186/1743-8977-8-1>
- S. Wang, D.K. Wang, S. Smart, J. Diniz da Costa, Ternary phase-separation investigation of sol-gel derived silica from ethyl silicate 40. *Sci Rep* **5**, 1–11 (2015). <https://doi.org/10.1038/srep14560>
- J.L. Montaña-Priede, J.P. Coelho, A. Guerrero-Martínez, O. Peña-Rodríguez, U. Pal, Fabrication of monodisperse Au@SiO₂ nanoparticles with highly stable silica layers by ultrasound-assisted Stöber method. *J Phys Chem C* **121**(17), 9543–9551 (2017). <https://doi.org/10.1021/acs.jpcc.7b00933>
- I.A. Rhaman, P. Vejayakumaran, C.S. Sipaut, J. Ismail, A. Bakar, R. Adnan, C.K. Chee, An optimized sol-gel synthesis of stable primary equivalent silica particles. *Colloids Surf A* **294**, 102–110 (2007). <https://doi.org/10.1016/j.colsurfa.2006.08.001>
- V. Lenart, N. Astrath, R. Turchiello, G. Goya, S. Gómez, Thermal diffusivity of ferrofluids as a function of particle size determined using the mode-mismatched dual-beam thermal lens technique. *J Appl Phys* **123**(8), 1–4 (2018). <https://doi.org/10.1063/1.5017025>
- G.A. López-Muñoz, J.A. Balderas-López, J. Ortega-López, J.A. Pescador-Rojas, J. Santoyo-Salazar, Thermal diffusivity

- measurement for urchin-like gold nanofluids with different solvents, sizes and concentrations/shapes. *Nanoscale Res Lett* **7**(667), 1–7 (2012). <https://doi.org/10.1186/1556-276X-7-667>
31. I.A. Rhaman, P. Vejayakumaran, C.S. Sipaut, J. Ismail, C.K. Chee, Size-dependent physicochemical and optical properties of silica nanoparticles. *Mater Chem Phys* **114**, 328–332 (2009). <https://doi.org/10.1016/j.matchemphys.2008.09.068>
 32. D.H. Kumar, H.E. Patel, V.R.R. Umar, T. Sundararajan, T. Pradeep, S. Das, Model for heat conduction in nanofluids. *Phys Rev Lett* **93**(14), 1–4 (2004)
 33. Z. Zheng, L. Qiu, G. Su, D. Tang, Y. Liao, C. Yunfa, Thermal conductivity and thermal diffusivity of SiO₂ nanopowder. *J Nanopart Res* **13**(12), 6887–6893 (2011). <https://doi.org/10.1007/s11051-011-0596-4>

Publisher's Note Springer Nature remains neutral with regard to jurisdictional claims in published maps and institutional affiliations.